

# Strong electron-phonon coupling and predicted highest known $T_c$ of MXenes revealed in 2H-Mo<sub>2</sub>N under biaxial stress

Komsilp Kotmool,<sup>\*,†,‡</sup> Prutthipong Tsuppayakorn-ae,<sup>†,§</sup> Thiti Bovornratanaraks,<sup>†,§</sup>  
Thanayut Kaewmaraya,<sup>||</sup> Rajeev Ahuja,<sup>#,®</sup> and Wei Luo<sup>#</sup>

<sup>†</sup>*College of Advanced Manufacturing Innovation, King Mongkut's Institute of Technology  
Ladkrabang, Bangkok 10520, Thailand*

<sup>‡</sup>*Electronic and Optoelectronic Device Research Unit, School of Science, King  
Mongkut's Institute of Technology Ladkrabang, Bangkok 10520, Thailand*

<sup>†</sup>*Extreme Condition Physics Research Laboratory, Physics of Energy Materials  
Research*

*Unit, Department of Physics, Faculty of Science, Chulalongkorn University, Bangkok,  
10330, Thailand*

<sup>§</sup>*Thailand Center of Excellence in Physics, Ministry of Higher Education, Science,  
Research and Innovation, 328 Si Ayutthaya Road, Bangkok, 10400, Thailand*

<sup>||</sup>*Integrated Nanotechnology Research Center, Department of Physics, Khon Kaen  
University, Khon Kaen, Thailand*

<sup>⊥</sup>*Institute of Nanomaterials Research and Innovation for Energy (IN-RIE),  
NANOTEC-KKU RNN on Nanomaterials Research and Innovation for Energy,  
KhonKaen University, Khon Kaen, 40002, Thailand*

<sup>#</sup>*Condensed Matter Theory Group, Materials Theory Division, Department of Physics  
and Astronomy, Uppsala University, Box 516, SE-75120, Uppsala, Sweden*

<sup>®</sup>*Department of Physics, Indian Institute of Technology (IIT), Ropar, Rupnagar  
140001, Punjab, India*

E-mail: komsilp.ko@kmitl.ac.th

Phone: +66 (0)2329 8264

## Abstract

Superconducting Mo-based MXenes have been intensively investigated because they possess the superior  $T_c$  values compared to other MXenes. This letter reports the unexpectedly strong electron-phonon coupling (EPC) and the highest  $T_c$  record ( $\approx 52$  K) among the MXenes revealed in the 2H-Mo<sub>2</sub>N under biaxial stress. At first, its excellent mechanical properties, including high ideal strength and elastic modulus, are demonstrated. Subsequently, EPC and corresponding  $T_c$  are elucidated upon the dynamically stable range of strain. For strain-free 2H-Mo<sub>2</sub>N, the EPC constant ( $\lambda$ ) and  $T_c$  are 1.3 and 22.7 K, respectively. The material exhibits remarkable enhancement in  $\lambda$  and  $T_c$  when subject to compressive and tensile stresses. The  $\lambda$  is approximately 2.2 at strains of -2.5% and 5%, yielding  $T_c$ 's of 52.1 and 25.3 K, respectively. Our findings suggest that the strain-dependent feature and energy levels of electronic bands play an essential role in enhancing EPC in 2H-Mo<sub>2</sub>N. This work paves the way for designing the MXene-based superconducting materials using strain engineering.

## Introduction

Superconductivity is a physical phenomenon in which the electric current can flow through a superconducting material with zero resistance below a specific superconducting critical temperature ( $T_c$ ). The Bardeen-Cooper-Schrieffer (BCS)-type superconductors have been successfully described by the electron-phonon coupling (EPC), which creates the Cooper pairs. After MgB<sub>2</sub> was discovered to possess the  $T_c$  of 39 K,<sup>1,2</sup> one feasible route of hunting the high- $T_c$  conventional superconductors is to consider the two-dimensional (2D) superconducting materials. Significant discoveries such as NbSe<sub>2</sub> few layers (3 - 7 K),<sup>3,4</sup> MgB<sub>2</sub> monolayer (20 K),<sup>5</sup> Mg<sub>2</sub>B<sub>4</sub>C<sub>2</sub> monolayer (47 K),<sup>6</sup> and hydrogenated MgB<sub>2</sub> monolayer (67 K)<sup>7</sup> have been reported. The advantage of this path is more practical than that of the rare-earth polyhydrides, which must be operated at extremely high pressure to attain the high- $T_c$ .<sup>8-11</sup>

Mo<sub>2</sub>X-based MXenes (X = C and N) have been attractive because they possess many promising properties, such as visible-light photocatalysis for H<sub>2</sub> production,<sup>11</sup> thermoelectricity,<sup>12,13</sup> electrochemical catalysis,<sup>14-17</sup> and energy storage.<sup>18,19</sup> Moreover, Mo<sub>2</sub>C and Mo<sub>2</sub>N exhibit superconducting materials with significantly high  $T_c$  among the MXene members. Experimentally, 2D ultrathin  $\alpha$ -Mo<sub>2</sub>C was successfully synthesized with  $T_c$  around 3 K.<sup>20</sup> Its  $T_c$  proportionally depends on sample thickness. As suggested by *ab initio* calculations, two monolayers are possible, namely tetragonal (1T) and hexagonal (2H) structures. The 2H has been proposed to be more energetically favorable in both Mo<sub>2</sub>C and Mo<sub>2</sub>N.<sup>21-23</sup> These two phases differ by the position of a Mo atom as described in the literature.<sup>21</sup> The  $T_c$  values of 1T and 2H of Mo<sub>2</sub>C were calculated to be 7.1 K<sup>24</sup> and 3.2 K,<sup>25</sup> respectively. These suggest that the  $T_c$  of 2H-Mo<sub>2</sub>C is more compatible with the experiment than that of another. For instance, the  $T_c$  of 1T-Mo<sub>2</sub>N was theoretically reported as 16 K.<sup>24</sup> Interestingly, replacing C with N can enhance the  $T_c$  of the 1T-Mo<sub>2</sub>X more than two times. As mentioned above, however, 2H-Mo<sub>2</sub>N as the most stable phase has not yet been investigated in terms of superconductivity.

Incorporating the strain engineering into MXenes enables tuning the electronic band structures, which intrinsically changes physical properties. For example, the spin-gapless semiconductor of Ti<sub>2</sub>C could be induced by biaxial strain ( $\epsilon$ ) over 2%. Compressive strain causes the semiconductor-to-metal transitions of Hf<sub>2</sub>CO<sub>2</sub> and Zr<sub>2</sub>CO<sub>2</sub>. The transitions of the indirect-to-direct bandgap of M<sub>2</sub>CO<sub>2</sub> (M=Sc, Ti, and Cr) can be attained by applying biaxial stress. Moreover, the  $T_c$  of Nb<sub>2</sub>CO<sub>2</sub> is increased by 4 K under applying a biaxial tensile strain of 4%. Hence, the application of strain results in profound consequences on the superconductivity of MXenes. Herein, this work investigates the strain-dependent  $T_c$  of 2H-Mo<sub>2</sub>N using density functional theory (DFT). The structural, mechanical, and electronic properties are also calculated. This theoretical study raises the feasible route of developing the MXene-based superconductor.

## Computational details

The vacuum-slab model, stress-strain response, and mechanical properties were performed following Ref.<sup>22</sup> We used the CASTEP code<sup>26</sup> with ultrasoft pseudopotential<sup>27</sup> as the electronic configurations of Mo:  $4s^2 4p^6 4d^5 5s^1$  and N:  $2s^2 2p^3$  under GGA-PBE scheme.<sup>28</sup> A dense Brillouin-zone (BZ) sampling grid of spacing  $0.04 \times 2\pi \text{ \AA}^{-1}$  and an  $E_{cut} = 500 \text{ eV}$  were verified for the sufficiently accurate geometry optimizations. The van der Waals (vdW) dispersion within Grimm's scheme<sup>29</sup> was included in calculating almost all calculations except the phonon dispersions. Phonon dispersion was performed based on supercell and finite displacement approaches with more accurate calculation ( $5 \times 10^{-8} \text{ eV/atom}$  and  $0.001 \text{ eV/\AA}$  for energetic and force convergence) to confirm the dynamic stability. The phonon-mediated superconductivity was investigated using the isotropic Eliashberg theory, as implemented in the Quantum Espresso (QE) code.<sup>30</sup> The  $E_{cut}$  for the plane-wave basis set was 80 Ry. The EPC matrix elements were computed in the first Brillouin zone (BZ) with  $8 \times 8 \times 1$  q-meshes, while the individual EPC matrices were sampled with  $64 \times 64 \times 4$  k-points mesh. A Gaussian broadening parameter of 0.12 Ry was used for the integration over the Fermi surface to evaluate the electron-phonon interaction. The Fermi surface was visualized using the FermiSurfer code.<sup>31</sup>  $T_c$  value was calculated by solving the Allen–Dynes equation [46] for  $\lambda < 1.5$ , and the  $T_{cs}$  of strong EPC ( $\lambda > 1.5$ ) was obtained by a modified theory ( $T_{cs} = f_1 f_2 T_c$ ),<sup>32</sup> as also seen full detail in Appendix of Ref.<sup>33</sup> Coulomb pseudopotential parameter ( $\mu^*$ ) was set to be 0.10.

## Results and discussion

Initially, the energetic stability of 1T- and 2H-Mo<sub>2</sub>N is investigated. The 2H phase is more stable than the 1T counterpart because of having lower energy by 90 meV/atom, agreeing with the reported studies.<sup>34</sup> This indicates that the 2H-Mo<sub>2</sub>N is more practical than another. The 2H-Mo<sub>2</sub>N has a lattice constant ( $a$ ) of  $2.818 \text{ \AA}$  and a thickness ( $d$ ) of  $5.442 \text{ \AA}$  at 0% strain.

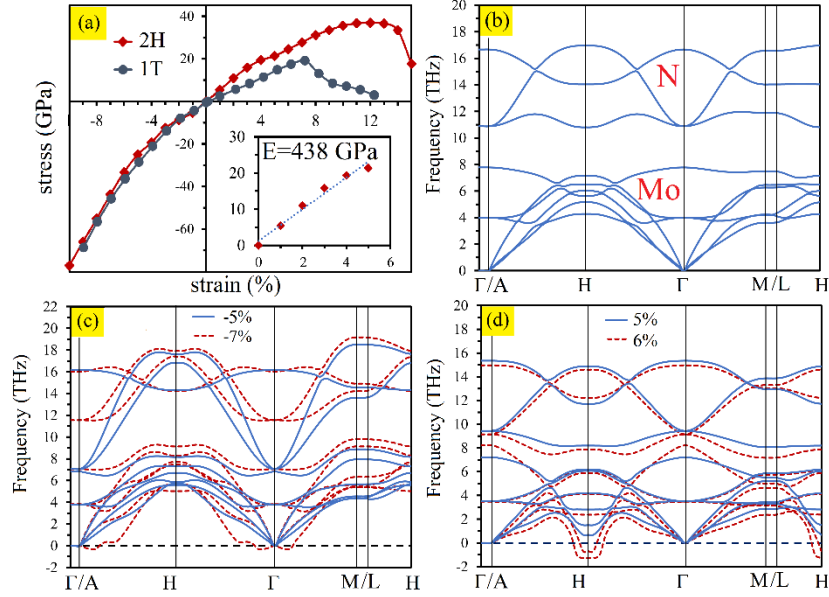


Figure 1: Stress-strain responses of the 2H-Mo<sub>2</sub>N and 1T-Mo<sub>2</sub>N (a), and the inset shows the linear fitting for evaluating elastic modulus. Phonon dispersion at unstressed condition (b), at compressive strains of -5% and -7% (c), and at tensile strains of 5% and 6% (d).

Subsequently, the stress-strain response shown in Fig. 1a provides the ideal stress (i.e.,  $\sigma_{max}$ ) of 37 GPa at 12% strain and elastic modulus (E) of 438 GPa, which is significantly high regarding those of the 1T-Mo<sub>2</sub>N ( $\sigma_{max}$ =19 GPa at 7% and E = 292 GPa). These comparative enhancements of mechanical properties of 2H-Mo<sub>2</sub>N are attributed by the different positions of a Mo atom respecting another, similar to the case of Mo<sub>2</sub>C<sup>22</sup> and W<sub>2</sub>C.<sup>35</sup> The dynamical stability of 2H phase is insisted in the unstressed structure as displayed in Fig. 1b. The vibrations of Mo atoms dominate at low frequencies up to 8 THz, whereas those of N atoms contribute at higher frequency range of 11-17 THz. Stable regimes both compressive and tensile strains are evaluated (Fig. 1c and 1d), as it is stable in the strain range of -5% to 5%. However, a slightly difference in the other approach—linear response deriving during the EPC calculations in next part obtains a stable range of -4% to 5% strain. Hence we will continually calculate further properties on this strain range.

The electronic band structure (EBS) as shown in Fig. 2a verifies the insignificant effect of spin-orbit coupling (SOC), corresponding with the previous studies in 1T-Mo<sub>2</sub>N.<sup>24</sup> Therefore,

the SOC will not be included into further calculations. The partial density of states (PDOS) reveals that around the Fermi level (FL) is mainly dominated by the 4d-Mo states. Moreover, minor distributions the 5s-Mo and 4p-Mo states are below the FL, and 2p-N states are above the FL. One can see the FL of the unstressed 2H-Mo<sub>2</sub>N is located nearby the local minimum of the total DOS valley. Consequently, the FL is expected to be easily tuned to higher electronic densities. Applying strain strongly affects band structures respecting the referent bands at  $\varepsilon = 0\%$ , as seen in Fig. 2b-e. At the tensile strain of 5%, the high-energetic valence band is enhanced to higher energies at H point, and the low-energetic conduction bands are stretched out with having lowest touching point with the FL at H point. Meanwhile, at compressive strains, the valence bands at H point are decreased to lower energy but those at the  $\Gamma$  point are pushed up to the FL.

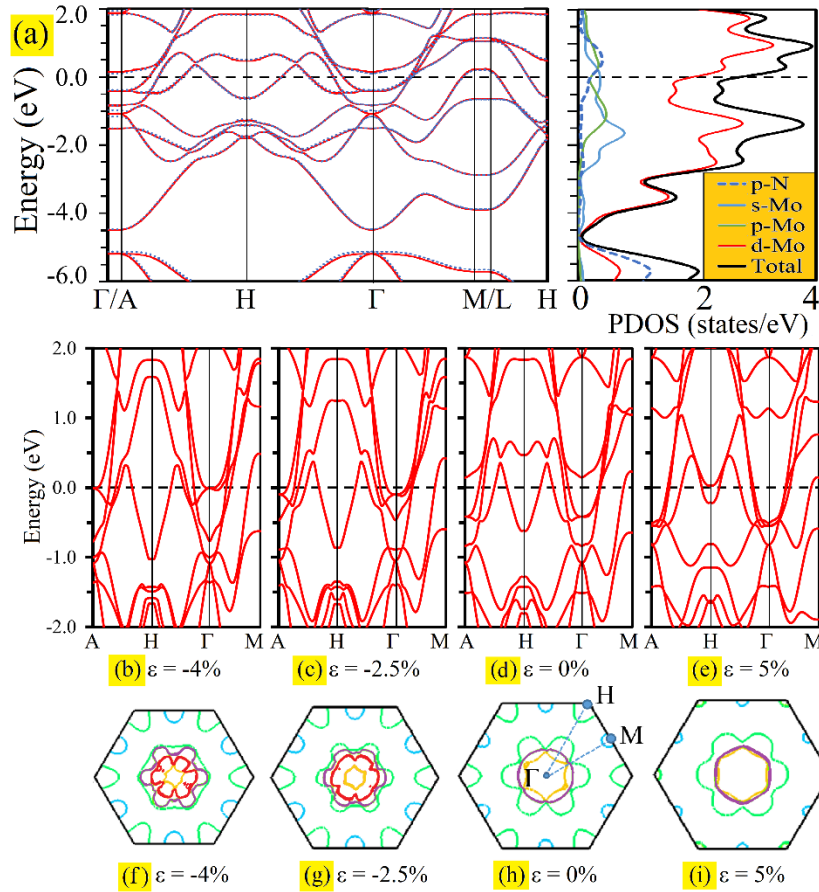


Figure 2: EBS and PDOS at (a) unstressed condition with SOC (solid-red line) and without SOC (dot-blue line), and strain-dependent EBS and Fermi surface at -4% (b, f), -2.5% (c, g), 0% (d, h), and 5% (e, i).

To gain insights into the electronic distribution around the FL, the Fermi surfaces (FS) of 2H-Mo<sub>2</sub>N are visualized at varying strains, as shown in Fig. 3f-i. At the reference of  $\varepsilon = 0\%$ , FS consists of five distinctly different pockets: (i) a pancake-type electron pocket, (ii) a larger circle electron pocket, and (iii) a nest electron pocket around  $\Gamma$  point, (iv) six-hole type pockets around K point, and (v) six-hole type pockets around M point, as seen in Fig. 2h. At a tensile strain of 5% (Fig. 2i), pocket (i) significantly extends and nearly touches pocket (ii), and pocket (iii) climbs moderately. Moreover, pockets (iv) and (v) are dramatically declined respecting to  $\varepsilon = 0\%$ . At the compressive strains of -2.5% (Fig. 2g) and 4% (Fig. 2f), pocket (i) is gradually decreased, and pocket (ii) is transformed to be a nest. Interestingly, an additional nest electron pocket emerges around  $\Gamma$  point, corresponding with a sinking band at this zone. Furthermore, pocket (iii) is moderately reshaped to be a like-hexagon shape at -4%. It is worth noting that the FS has one more electron pocket around  $\Gamma$  at compressive strains. The presence of magnitude of both the electron and hole pockets can be attributed to the enhancement of  $T_c$  through a strain-induced electronic topological transition. Also, the band features and FS at calculated strains reflect the numbers of electron density at Fermi level ( $N_{Ef}$ ) depicted in Fig. 4a. Interestingly, it is found that the  $N_{Ef}$  can be enhanced by both tensile and compressive stresses, as a sequence of the possibility of increasing electron-phonon coupling (EPC) of this material at certain biaxial strains.

The  $T_c$  values of 2H phase versus biaxial strains are calculated using the Allen-Dynes formula. This formula needs the input parameters, including the integration of the  $\lambda(\omega)$  and the logarithmic average of the spectral function ( $\omega_{log}$ ) which are solved by the isotropic Eliashberg theory, as obeyed by equations 1 to 3.

$$T_c = \frac{\omega_{log}}{1.2} \exp \left[ -\frac{1.04(1+\lambda)}{\lambda - \mu^* (1+0.62\lambda)} \right] \quad (1)$$

$$\lambda = 2 \int_0^{\infty} \frac{d\omega}{\omega} \alpha^2 F(\omega) \quad (2)$$

$$\omega_{log} = \exp \left( \frac{2}{\lambda} \int_0^{\infty} \frac{d\omega}{\omega} \alpha^2 F(\omega) \ln \omega \right) \quad (3)$$

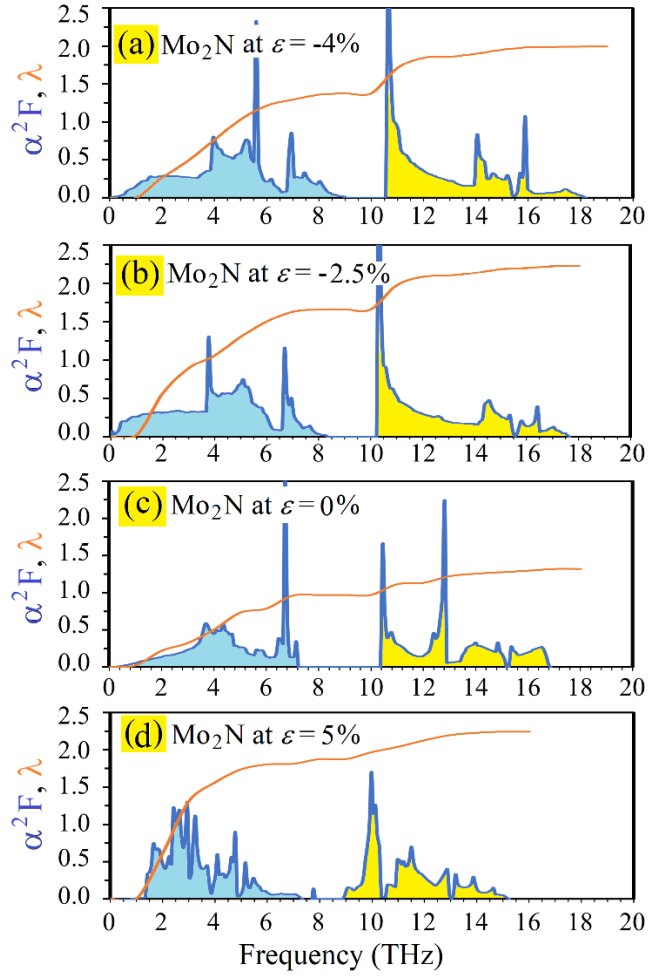


Figure 3: The  $\alpha^2 F(\omega)$ ,  $\lambda$ , and FS at -4% (a), -2.5% (b), 0% (c), and 5% (d) of 2H-Mo2. The blue and yellow shades represent the coupling modes with vibrations of Mo and N atoms, respectively.

where  $\alpha^2F(\omega)$  is the Eliashberg spectral function. Unexpectedly, the phonon spectrum determined by the linear-response approach at -5% strain contains the enormous negative frequencies which is unable to process the EPC. Therefore, it is the reason why the strain range of -4% to 5% are chosen to investigate the superconductive property.

The  $\alpha^2F(\omega)$  patterns of 2H-Mo<sub>2</sub>N at calculated strains have a gap between the spectra contributed by vibrations of Mo and N atoms. The frequency distribution of  $\alpha^2F(\omega)$  depends on the interaction between atoms, stretching out to higher frequency from tensioned to compressed structures. At the unstressed structure, it has the widest gap and has a  $\lambda$  of 1.32 as displayed in Fig. 3c. Intriguingly, Fig. 3a, 3b, and 3d demonstrate that the  $\lambda$  values of 2H-Mo<sub>2</sub>N at -4%, -2.5%, and 5% strains are 2.00, 2.23, and 2.24, respectively. These values are classified to be the behavior of strong electron-phonon coupling ( $\lambda > 1.5$ ). This finding is the first theoretical study, that uncovers the existence of strong EPC in the MXene family and metal nitrides.

Here we plot the related superconductive parameters as a function of strain in Fig. 4a-b to clarify their strain dependencies. At 0% strain, the  $\omega_{log}$  and  $T_c$  of 2H-Mo<sub>2</sub>N are 227 cm<sup>-1</sup> and 22.7 K, respectively. This  $T_c$  value is higher than the  $T_c$  of 1T-Mo<sub>2</sub>N ( $T_c = 16.8$  K) that is calculated in this work to validate the result of previous work ( $T_c = 16.0$  K) that used different pseudopotential and setting parameters.<sup>24</sup> It is essential to mention that the  $T_c$  of bare 2H-Mo<sub>2</sub>N is significantly high compared to those of other MXenes without surface functionalization and applying external stresses. At -2.5% and 5% strains, the  $\omega_{log}$  inversely relates with the  $N_{Ef}$ . It can be explicitly explained by equation 2 that the  $\omega_{log}$  should be decreased with increasing  $\lambda$ . The  $T_c$  values of the 2H-Mo<sub>2</sub>N solved by equation 1 are 34.5,

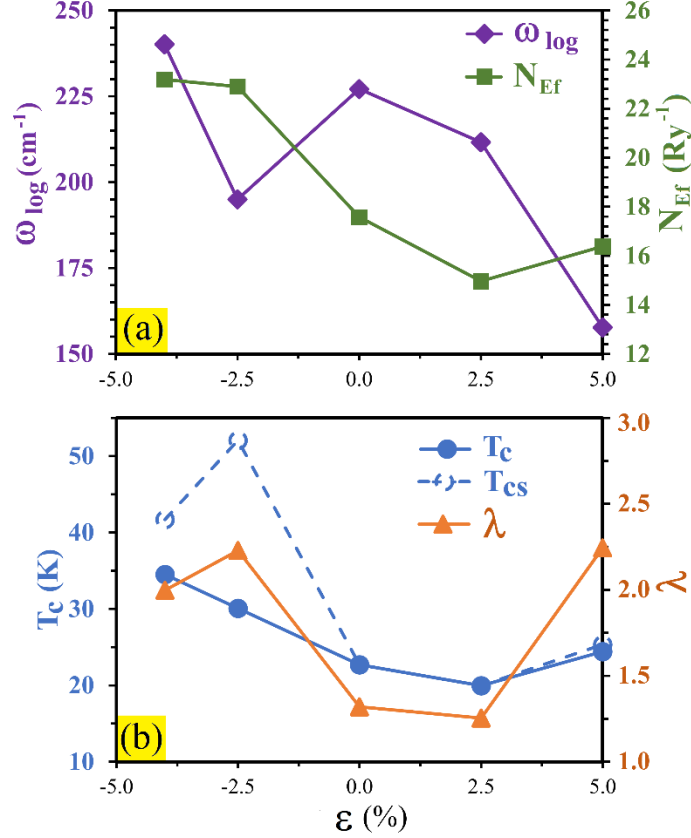


Figure 4: (a) The  $\omega_{log}$  and  $N_{Ef}$ , and (b) the  $T_c$ ,  $T_{cs}$ , and  $\lambda$  of 2H-Mo<sub>2</sub>N as a function of strain.

30.1, and 24.4 K for strains of -4%, -2.5%, and 5%, respectively. According to the strong EPC at these strain values, it is important to include the correction factors ( $f_1$  and  $f_2$ ) for obtaining a more plausible superconducting temperature ( $T_{cs}=f_1f_2.T_c$ ). We find that the tendency of  $T_{cs}$  is more consistent with  $\lambda$  than that of  $T_c$ , as shown in Fig. 4b. The  $T_{cs}$  values are 41.7, 52.1, and 25.3 K for strains of -4%, -2.5%, and 5%, respectively. It is worth noting that the  $T_{cs}$  of the 2H-Mo<sub>2</sub>N at -2.5% strain is the highest value among those of reported MXene members.

## Conclusion

In summary, this letter reveals an unexpectedly strong electron-phonon coupling (EPC) in 2H-Mo<sub>2</sub>N under biaxial stress. The 2H-Mo<sub>2</sub>N is considered because it is more energetically stable than another structure, 1T-Mo<sub>2</sub>N. It processes to be dynamically stable structure

in the wide strain range of -4% to 5%. Application of stress plays an essential role in tuning both feature and energy level of electronic band structure (EBS), consequently enhancing EPC. The EBS, FS, and  $N_{Ef}$  are carefully elucidated to advocate a strong EPC. The corrected critical temperature for strong EPC,  $T_{cs}$ , is evaluated as 41.7, 52.1, and 25.3K for strains of -4%, -2.5%, and 5%, respectively. Our finding provides a new record for the highest  $T_c$  among the MXene family. This result challenges the further experiment to prove it and paves the guidance for developing the MXene-based superconductor for modern material applications.

This work was supported by the King Mongkut's Institute of Technology Ladkrabang (KMITL) under the Fundamental Fund (contract number: KRIS/FF65/25). The computing facilities are provided by the College of Advanced Manufacturing Innovation (AMI), SNIC(2021/1-42) and SNAC of Sweden are acknowledged for providing part of the computing facilities. Authors also gratefully acknowledge the Swedish Research Council (VR-2016-06014 VR-2020-04410) for financial support.

## References

- (1) Nagamatsu, J.; Nakagawa, N.; Muranaka, T.; Zenitani, Y.; Akimitsu, J. Superconductivity at 39 K in magnesium diboride. *nature* **2001**, *410*, 63–64.
- (2) Choi, H. J.; Roundy, D.; Sun, H.; Cohen, M. L.; Louie, S. G. The origin of the anomaloussuperconducting properties of MgB<sub>2</sub>. *Nature* **2002**, *418*, 758–760.

- (3) Frindt, R. F. Superconductivity in Ultrathin NbSe<sub>2</sub> Layers. *Phys. Rev. Lett.* **1972**, *28*, 299–301.
- (4) Xi, X.; Wang, Z.; Zhao, W.; Park, J.-H.; Law, K. T.; Berger, H.; Forró, L.; Shan, J.; Mak, K. F. Ising pairing in superconducting NbSe<sub>2</sub> atomic layers. *Nature Physics* **2016**, *12*, 139–143.
- (5) Bekaert, J.; Aperis, A.; Partoens, B.; Oppeneer, P. M.; Milošević, M. V. Evolution of multigap superconductivity in the atomically thin limit: Strain-enhanced three-gap superconductivity in monolayer MgB<sub>2</sub>. *Phys. Rev. B* **2017**, *96*, 094510.
- (6) Singh, S.; Romero, A. H.; Mella, J. D.; Ereameev, V.; Muñoz, E.; Alexandrova, A. N.; Rabe, K. M.; Vanderbilt, D.; Muñoz, F. High-temperature phonon-mediated superconductivity in monolayer Mg<sub>2</sub>B<sub>4</sub>C<sub>2</sub>. *npj Quantum Materials* **2022**, *7*, 1–8.
- (7) Bekaert, J.; Petrov, M.; Aperis, A.; Oppeneer, P. M.; Milošević, M. Hydrogen-Induced high-temperature superconductivity in two-dimensional materials: the example of hydrogenated monolayer MgB<sub>2</sub>. *Physical review letters* **2019**, *123*, 077001.
- (8) Zhong, X.; Wang, H.; Zhang, J.; Liu, H.; Zhang, S.; Song, H.-F.; Yang, G.; Zhang, L.; Ma, Y. Tellurium hydrides at high pressures: High-temperature superconductors. *Physical review letters* **2016**, *116*, 057002.
- (9) Drozdov, A.; Kong, P.; Minkov, V.; Besedin, S.; Kuzovnikov, M.; Mozaffari, S.; Balicas, L.; Balakirev, F.; Graf, D.; Prakapenka, V., et al. Superconductivity at 250 K in lanthanum hydride under high pressures. *Nature* **2019**, *569*, 528–531.
- (10) Somayazulu, M.; Ahart, M.; Mishra, A. K.; Geballe, Z. M.; Baldini, M.; Meng, Y.; Struzhkin, V. V.; Hemley, R. J. Evidence for superconductivity above 260 K in lanthanum superhydride at megabar pressures. *Physical review letters* **2019**, *122*, 027001.

- (11) Peng, F.; Sun, Y.; Pickard, C. J.; Needs, R. J.; Wu, Q.; Ma, Y. Hydrogen clathrate structures in rare earth hydrides at high pressures: possible route to room-temperature superconductivity. *Physical review letters* **2017**, *119*, 107001.
- (12) Khazaei, M.; Arai, M.; Sasaki, T.; Estili, M.; Sakka, Y. Two-dimensional molybdenum carbides: potential thermoelectric materials of the MXene family. *Physical Chemistry Chemical Physics* **2014**, *16*, 7841–7849.
- (13) Kim, H.; Anasori, B.; Gogotsi, Y.; Alshareef, H. N. Thermoelectric properties of two-dimensional molybdenum-based MXenes. *Chemistry of Materials* **2017**, *29*, 6472–6479.
- (14) Du, C.; Huang, H.; Wu, Y.; Wu, S.; Song, W. Ultra-efficient electrocatalytic hydrogen evolution at one-step carbonization generated molybdenum carbide nanosheets/N-doped carbon. *Nanoscale* **2016**, *8*, 16251–16258.
- (15) Seh, Z. W.; Fredrickson, K. D.; Anasori, B.; Kibsgaard, J.; Strickler, A. L.; Lukatskaya, M. R.; Gogotsi, Y.; Jaramillo, T. F.; Vojvodic, A. Two-dimensional molybdenum carbide (MXene) as an efficient electrocatalyst for hydrogen evolution. *ACS Energy Letters* **2016**, *1*, 589–594.
- (16) Handoko, A. D.; Fredrickson, K. D.; Anasori, B.; Convey, K. W.; Johnson, L. R.; Gogotsi, Y.; Vojvodic, A.; Seh, Z. W. Tuning the basal plane functionalization of two-dimensional metal carbides (MXenes) to control hydrogen evolution activity. *ACS Applied Energy Materials* **2017**, *1*, 173–180.
- (17) Cheng, Z.; Fu, Q.; Han, Q.; Xiao, Y.; Liang, Y.; Zhao, Y.; Qu, L. A type of 1 nm molybdenum carbide confined within carbon nanomesh as highly efficient bifunctional electrocatalyst. *Advanced Functional Materials* **2018**, *28*, 1705967.
- (18) Halim, J.; Kota, S.; Lukatskaya, M. R.; Naguib, M.; Zhao, M.-Q.; Moon, E. J.; Pitock, J.; Nanda, J.; May, S. J.; Gogotsi, Y., et al. Synthesis and characterization

- of 2D molybdenum carbide (MXene). *Advanced Functional Materials* **2016**, *26*, 3118–3127.
- (19) Sun, Q.; Dai, Y.; Ma, Y.; Jing, T.; Wei, W.; Huang, B. Ab initio prediction and characterization of Mo<sub>2</sub>C monolayer as anodes for lithium-ion and sodium-ion batteries. *The journal of physical chemistry letters* **2016**, *7*, 937–943.
- (20) Xu, C.; Wang, L.; Liu, Z.; Chen, L.; Guo, J.; Kang, N.; Ma, X.-L.; Cheng, H.-M.; Ren, W. Large-area high-quality 2D ultrathin Mo<sub>2</sub>C superconducting crystals. *Nature materials* **2015**, *14*, 1135–1141.
- (21) Sun, W.; Li, Y.; Wang, B.; Jiang, X.; Katsnelson, M. I.; Korzhavyi, P.; Eriksson, O.; Di Marco, I. A new 2D monolayer BiXene, M<sub>2</sub>C (M = Mo, Tc, Os). *Nanoscale* **2016**, *8*, 15753–15762.
- (22) Kotmool, K.; Kaewmaraya, T.; Hussain, T.; Ahuja, R.; Luo, W.; Bovornratanaraks, T. Biaxial stress and functional groups (T = O, F, and Cl) tuning the structural, mechanical, and electronic properties of monolayer molybdenum carbide. *Physical Chemistry Chemical Physics* **2022**, DOI:10.1039/d2cp02557d.
- (23) Jin, W.; Wu, S.; Wang, Z. Structural, electronic and mechanical properties of two-dimensional Janus transition metal carbides and nitrides. *Physica E: Low-dimensional Systems and Nanostructures* **2018**, *103*, 307–313.
- (24) Bekaert, J.; Sevik, C.; Milošević, M. V. First-principles exploration of superconductivity in MXenes. *Nanoscale* **2020**, *12*, 17354–17361.
- (25) Lei, J.; Kutana, A.; Yakobson, B. I. Predicting stable phase monolayer Mo<sub>2</sub>C (MXene), a superconductor with chemically-tunable critical temperature. *J. Mater. Chem. C* **2017**, *5*, 3438–3444.

- (26) Clark, S. J.; Segall, M. D.; Pickard, C. J.; Hasnip, P. J.; Probert, M. I.; Refson, K.; Payne, M. C. First principles methods using CASTEP. *Z. Kristallogr. Cryst. Mater.* **2005**, *220*, 567–570.
- (27) Vanderbilt, D. Soft self-consistent pseudopotentials in a generalized eigenvalue formalism. *Phys. Rev. B* **1990**, *41*, 7892–7895.
- (28) Perdew, J. P.; Burke, K.; Ernzerhof, M. Generalized Gradient Approximation Made Simple. *Phys. Rev. Lett.* **1996**, *77*, 3865–3868.
- (29) Grimme, S. Semiempirical GGA-type density functional constructed with a long-range dispersion correction. *Journal of Computational Chemistry* **2006**, *27*, 1787–1799.
- (30) Giannozzi, P.; Baroni, S.; Bonini, N.; Calandra, M.; Car, R.; Cavazzoni, C.; Ceresoli, D.; Chiarotti, G. L.; Cococcioni, M.; Dabo, I.; et al., QUANTUM ESPRESSO: a modular and open-source software project for quantum simulations of materials. *J. Phys. Condens. Matter* **2009**, *21*, 395502.
- (31) Kawamura, M. FermiSurfer: Fermi-surface viewer providing multiple representation schemes. *Computer Physics Communications* **2019**, *239*, 197–203.
- (32) Allen, P. B.; Dynes, R. C. Transition temperature of strong-coupled superconductors reanalyzed. *Phys. Rev. B* **1975**, *12*, 905–922.
- (33) Sukmas, W.; Tsuppayakorn-ae, P.; Pinsook, U.; Bovornratanaraks, T. Near-room-temperature superconductivity of Mg/Ca substituted metal hexahydride under pressure. *Journal of Alloys and Compounds* **2020**, *849*, 156434.
- (34) Jin, W.; Wu, S.; Wang, Z. Structural, electronic and mechanical properties of two-dimensional Janus transition metal carbides and nitrides. *Physica E: Low-dimensional Systems and Nanostructures* **2018**, *103*, 307–313.
- (35) Wang, J.; Bai, L.; Yao, C.; Niu, L. A DFT computational prediction of 2H phase W<sub>2</sub>C monolayer and the effect of O functional groups. *Physics Letters A* **2022**, *424*, 12784.